A map of chemical potential differences within an outcrop

JOHN M. FERRY

Department of Geology, Arizona State University
Tempe, Arizona 85281

Abstract

Mineral assemblages in different samples of metamorphosed argillaceous carbonate rock, collected from a single, large outcrop in south-central Maine, record differences in the chemical potentials of CO_2 and H_2O between samples during metamorphism. Because all samples contain graphite and pyrrhotite of constant composition, differences in the chemical potentials of O_2, H_2, CH_4, and H_2S existed as well. Thermodynamic analysis of the mineral assemblages indicates that maximum chemical potential differences were on the order of 100 calories. Maximum differences in the chemical potentials of FeO, MgO, K_2O, Al_2O_3, and CaO between samples are of approximately the same magnitude. The differences in chemical potentials of CO_2 and H_2O between beds, however, correspond to a difference of only a few hundredths X_{CO_2} in the composition of a CO_2–H_2O fluid in equilibrium with the samples. Maximum gradients in the chemical potentials of CO_2 and H_2O during metamorphism at the outcrop were 5–6 cal/m in magnitude.

Differences in chemical potentials of CO_2 and H_2O can be mapped in three dimensions in the outcrop, and they exhibit an extremely regular pattern. With the exception of one sample, there are no detectable differences in chemical potentials parallel to bedding and schistosity (which have identical orientations in the outcrop). All other differences occur between different beds. The mapped differences in chemical potentials can be used to quantitatively estimate upper bounds on mass transfer of CO_2 and H_2O during metamorphism at the outcrop. The estimated upper bounds on mass transfer are consistent with (but do not require) a model of channelized fluid transfer during metamorphism in which fluid transfer primarily occurs in directions parallel to bedding and schistosity.

Introduction

Metamorphism involves the liberation of CO_2 and H_2O from rocks, and there must exist during metamorphism some volatile-rich fluid (or fluid-like) phase containing CO_2 and H_2O. The volatile phase, however, is not preserved, except for rocks that contain fluid inclusions, and its behavior during metamorphism must be inferred from mineral equilibria. The classical model of metamorphism assumes that the fluid phase in any particular rock is in communication with some external agent that controls the fluid's composition. The composition of the volatile phase in an outcrop, therefore, is regarded to be controlled *externally* and hence to be *constant*. Petrologic investigations indicate that in some cases the classical model of metamorphism appears to be valid (Carmichael, 1970). Several studies, however, have concluded that variations in the composition of the vola-

tile phase exist within single outcrop-size areas during metamorphism (see, for example, James and Howland, 1955; Guidotti, 1970; Hewitt, 1973; Osberg, 1974a; Rumble, 1974, 1978). In addition, the study of metamorphosed carbonate rocks reveals that the composition of the fluid phase during the course of prograde metamorphism is to a large degree internally controlled by the rock's mineral assemblage rather than by some external agent (Hewitt, 1973; Greenwood, 1975; Ferry, 1976a; Rice, 1977a, b).

The classical model of metamorphism in some cases must be incorrect, and the behavior of the volatile phase during metamorphism should be reevaluated. Some aspects of the behavior of the volatile phase during metamorphism have been studied on a regional scale (Ferry, 1978a). Important constraints on the behavior of the fluid phase in metamorphic processes can also be deduced from the study of single outcrops that contain a variety of mineral as-

semblages. Rumble (1974, 1978) pioneered developments in the latter kind of study. Rumble's results apply to the behavior of O–H fluids in rocks that underwent dehydration during metamorphism. This report presents mineralogical and petrological data from a single, large outcrop of metamorphosed argillaceous carbonate rock that reveal aspects of the behavior of C–O–H–S fluids during metamorphism which involves simultaneous dehydration and decarbonation. Specifically the report (1) documents differences in the chemical potentials of CO_2 and H_2O in the volatile phase in the outcrop during metamorphism; (2) presents the geometric pattern of the chemical potential differences in three dimensions; (3) relates the pattern of chemical potential differences to the local structural geology; (4) interprets the pattern of chemical potential differences in terms of a model of fluid transfer during metamorphism in which transfer of fluids preferentially occurs in channelways parallel to bedding and schistosity.

Geological setting

Samples were collected in the limestone member of the Silurian Waterville Formation from the vertical walls of the Blue Rock Quarry in south-central Maine (Fig. 1), in the town of Sidney. The bedding in the quarry is vertical and strikes N25E. Compositional layering is on a scale of 1–8 cm. The age of the rocks, as well as the lack of reaction textures between minerals, suggests that the rocks were subjected to one metamorphic episode (corresponding to the Devonian Acadian Orogeny). Porphyroblasts of most minerals crosscut schistosity, which indicates that metamorphism followed all or almost all deformation. The grade of metamorphism in nearby pelitic schists corresponds to that of the garnet zone. The stratigraphy, structural geology, and the metamorphism of the pelitic schists have been discussed in more detail by Osberg (1968, 1971, 1974a, b); the metamorphism of the argillaceous carbonate rocks has been studied on a regional scale by Ferry (1976a, b).

Methods of investigation

Approximately 80 samples were collected from the quarry, and the location of samples within the quarry is diagrammed in Figure 2. The floor of the quarry is approximately 13 meters below ground surface. Figure 2 illustrates the size and shape of the quarry when samples were collected in 1976 and 1977. Since this time the quarry has been deepened approximately 3 meters and the north end extended approxi-

mately 25 meters. Two sets of samples were collected. The first set was collected parallel to the north face of the quarry along a 100-meter traverse that cut across bedding. These samples are identified by a "B" prefix. The numerical suffix corresponds to the distance in meters along the traverse (from at the quarry's west end) at which the sample was collected. The second set was collected from several beds exposed on the west face of the quarry. These samples are identified by a numerical prefix that identifies the bed. The alphabetical suffix refers to the location of the samples within the bed. Rock samples collected from individual beds are separated both in horizontal (N–S) and in vertical (up–down) dimensions.

Mineral assemblages in each sample were identified by both petrography and X-ray diffractometry. An assemblage of minerals was judged to be in equilibrium using the same criteria listed by Ferry (1976a). Compositions of minerals in approximately 40 samples were determined using the automated MAC electron microprobe at the Geophysical Laboratory (Finger and Hadidiacos, 1971), natural and synthetic carbonate and silicate mineral standards, and the MAGIC data reduction program (a ZAF correction scheme) at the Geophysical Laboratory microprobe facility.

Mineralogy and mineral chemistry

Observed mineral assemblages

All samples contain calcite, chlorite, quartz, plagioclase, pyrrhotite, biotite, and graphite. Five distinct mineral assemblages have been observed, differentiated by the mineral(s) associated with those above: (a) muscovite, (b) muscovite + ankerite, (c) calcic amphibole, (d) calcic amphibole + ankerite, (e) muscovite + garnet. The five mineral assemblages will be referred to in the remainder of the report by these identification letters.

Mineral chemistry

The composition of all minerals in 22 samples was determined by electron microprobe; the composition of chlorite and plagioclase in 19 additional samples was determined. Table 1 and Figures 3–4 summarize the compositions. Although the minerals contain up to seven oxide components, the variations in mineral compositions are surprisingly simple. Plagioclase is a binary albite–anorthite solid solution. Chlorite, calcite, ankerite, biotite, muscovite, and calcic amphibole may be considered binary Fe–Mg solid solutions
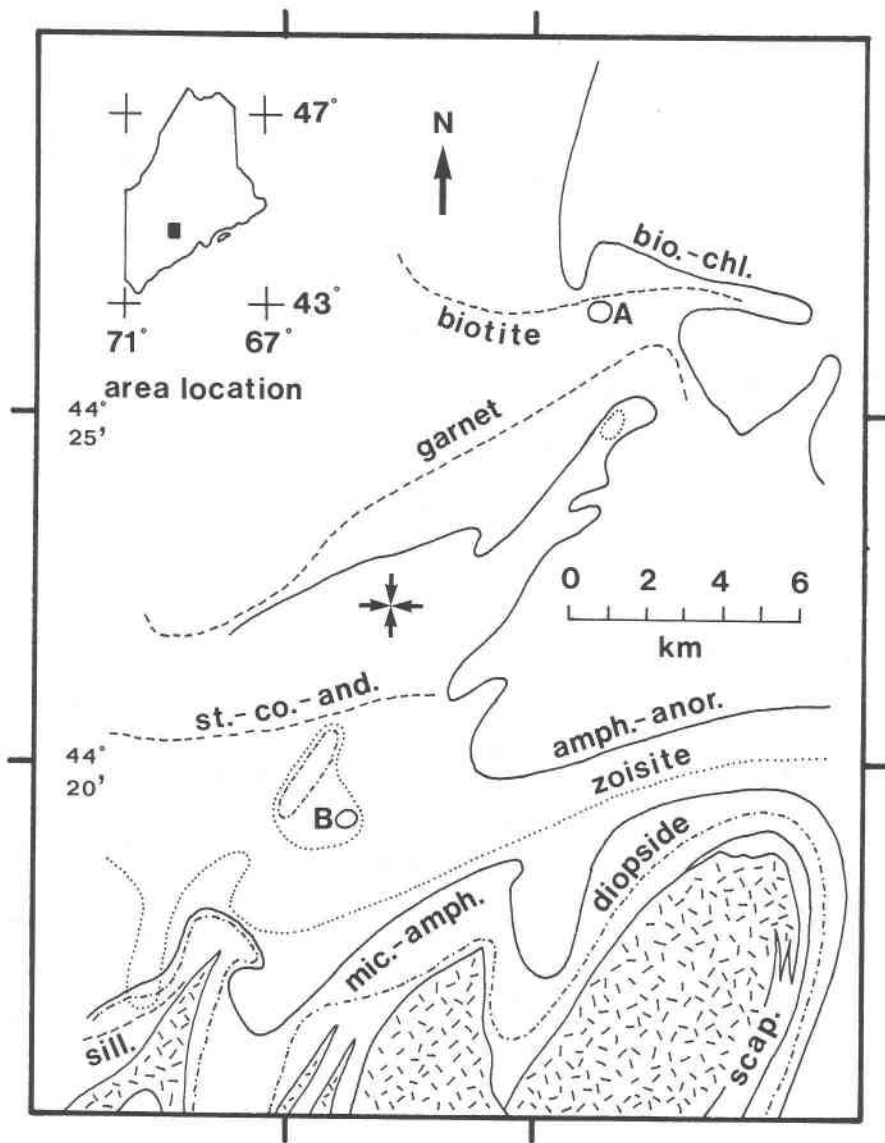
Fig. 1. Metamorphic sketch map of the Waterville–Vassalboro area, south-central Maine. Location of quarry described in this report is at the tips of the four opposed arrows. Dashed lines are isograds mapped by Osberg (1968, 1971) from mineral assemblages in pelitic schists (st.–co.–and. = staurolite–cordierite–andalusite isograd; sill. = sillimanite isograd). Other lines are isograds mapped by Ferry (1976a) from mineral assemblages in argillaceous metacarbonates. Solid lines: biotite–chlorite (bio.–chl.), amphibole–anorthite (amph.–anor., A), microcline–amphibole (mic.–amph., B), and scapolite (scap.) isograds; dotted line: zoisite isograd; dash–dot line: diopside isograd. Patterned areas are synmetamorphic granitic stocks.

with end-members and variations in Fe/(Fe + Mg) listed in Table 1A. Figure 3 illustrates compositions of all analyzed chlorite and biotite on a diagram that projects through SiO_2, H_2O, KAl_3O_5, and $NaAl_3O_5$ (i.e., considers minerals that coexist with quartz, H_2O-bearing fluid phase of constant μ_{H_2O}, and K–Na muscovite of fixed K/Na). Figure 3 demonstrates that chlorite and biotite minerals are close to binary Fe–Mg solid solutions, with compositions adequately

expressed by the structural formulas in Table 1A (represented by the solid horizontal lines in Fig. 3). Ankerite and amphibole compositions are illustrated in Figure 4. The coordinate of the apex of the figure is CaO when ankerite compositions (circles) are considered; the ankerite diagram projects through CO_2. Figure 4 demonstrates that ankerite in rocks from the quarry is close to a binary Fe–Mg compound whose formula is listed in Table 1A (and represented in Fig.
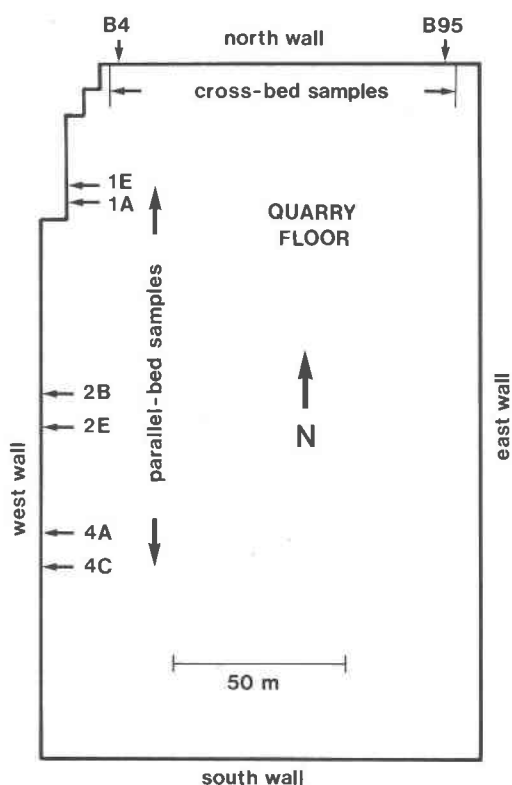
Fig. 2. Map of quarry. Lithologic layers are vertical and strike N25E. Two sets of samples were taken: one set across layering from the north side of the quarry (B4–B95); a second set parallel to beds 1, 2, and 4 on the west side of the quarry.

4 by the upper horizontal line). The coordinate of the apex of Figure 4 is Al_2O_3–CaO–Na_2O when amphibole compositions (crosses) are considered, and the amphibole diagram projects through SiO_2, H_2O, $NaAlO_2$, and $CaAl_2O_4$ (*i.e.*, considers minerals that coexist with quartz, an H_2O-bearing fluid phase of constant μ_{H_2O}, and plagioclase of fixed composition). Figure 4 demonstrates that amphiboles in the rocks of this study are close to binary Fe–Mg compounds with composition adequately expressed by the formula in Table 1A (represented by the lower horizontal line in Fig. 4). Additional compositional parameters of minerals that justify the choice of the mineral formulas in Table 1A are summarized in Table 1B.

The compositions of muscovite, biotite, chlorite, quartz, calcite, ankerite, plagioclase, calcic amphibole, pyrrhotite, and graphite may be adequately described by the system components MgO–FeO–CaO–Al_2O_3–K_2O–Na_2O–SiO_2–S–C–H_2O–CO_2. With the exception of plagioclase and quartz, all minerals contain minor MnO (less than 0.001 cation fraction) and all but plagioclase, quartz, and ankerite contain mi-

nor TiO_2 (less than 0.012 cation fraction). Although in the following thermodynamic treatment of the mineral assemblages, the Ti- and Mn-content of minerals is ignored, quantitative justification for doing so will be presented.

Garnets contain significant amounts of MnO, and, in addition, are Ca–Fe–Mg–Mn rather than simple Fe–Mg compounds. For this reason, garnet-bearing assemblages will not be considered beyond the discussion of biotite–garnet geothermometry.

Plagioclase occurs in the metacarbonate rocks as 10–100 μm multi-grain aggregates. While compositions of muscovite, chlorite, biotite, calcite, ankerite, and amphibole are remarkably constant in any one thin section, composition of 1–3 μm^2 areas within the plagioclase aggregates (determined by electron microprobe) varies *even within one aggregate* (greatest variation is between An_{31} and An_{64}). Plagioclase aggregates in any one sample, however are always either in the composition range An_{30}–An_{85} or in the composition range An_2–An_{30}. The composition data for plagioclase aggregates with bulk compositions in the range An_{30}–An_{85} are interpreted as follows: the plagioclase aggregates are intergrowths of two fine-grained feldspars, one $\sim An_{30}$ and the other $\sim An_{85}$. The existence of a miscibility gap in the plagioclase series between $\sim An_{30}$ and $\sim An_{85}$ at metamorphic conditions appropriate for the garnet zone has been predicted from crystallographic and crystal-chemical arguments by Smith (1975), and Smith's prediction is verified by studies of metamorphosed mafic igneous rocks (Voll, 1971; Spear, 1977a). In the treatment of the phase equilibria that follows, only rocks containing plagioclase aggregates with bulk composition An_{30}–An_{85} will be treated. Rock samples containing plagioclase aggregates with bulk composition An_2–An_{30} will not be considered further.

The composition of pyrrhotite in seven samples was determined by electron microprobe. Pyrrhotite is a binary FeS–S_2 solid solution with remarkably monotonous X_{FeS}: 0.945 ± 0.005, where the analytical error in the measurement of X_{FeS} is approximately ±0.01.

Attainment of equilibrium

Two observations can be used to evaluate the attainment of chemical equilibrium among mineral phases. First, no minerals are observed to have textures indicative of a reaction relationship. Second, Fe and Mg are partitioned in a very systematic fashion between pairs of Fe–Mg-bearing minerals (Table

Table 1. Mineral composition data

A. Structural formulas for minerals; Fe-Mg variations.

Mineral	Mineral symbol	Approximate structural formula (determined by electron microprobe)	Range in Fe/(Fe + Mg)
Quartz	Qz	SiO_2	··· ·
Graphite	Gr	C	···
Plagioclase	Pl	$(Na,Ca)(Al,Si)Si_2O_8$	···
Chlorite	Ch	$(Fe,Mg)_{4.68}Al_{2.64}Si_{2.68}O_{10}(OH)_8$	0.20 – 0.58
Biotite	Bi	$K_{0.9}(Fe,Mg)_{2.75}Al_{1.4}Si_{2.85}O_{10}(OH)_2$	0.24 – 0.62
Calcite	Cc	$Ca_{0.94}(Fe,Mg)_{0.06}CO_3$	0.26 – 0.52
Ankerite	Ak	$Ca(Fe,Mg)(CO_3)_2$	0.13 – 0.23
Muscovite	Mu	$K(Fe,Mg)_{0.1}Al_{2.8}Si_{3.1}O_{10}(OH)_2$	0.21 – 0.57
Calcic amphibole	Am	$\square_{0.9}Na_{0.1}(Ca_{1.9}Na_{0.1})\{(Fe,Mg)_{4.05}Al_{0.95}\}(Al_{0.95}Si_{7.05})O_{22}(OH)_2$	0.30 – 0.35

B. Additional compositional parameters of minerals that were used to devise the structural formulas in Table 1A.

Mineral	Compositional variable	Average value of variable (all analyzed minerals)	Standard deviation of variable
Biotite	$K/(K+Na+Ca+\square)$	0.871	0.039
Biotite	$\square/(K+Na+Ca+\square)$	0.105	0.040
Biotite	$Mn/(Fe+Mg+Mn+Ti+Al^{VI})$	0.001	<0.001
Biotite	$Ti/(Fe+Mg+Mn+Ti+Al^{VI})$	0.028	0.005
Muscovite	$K/(K+Na+Ca)$	0.933	0.011
Muscovite	$Mn/(Fe+Mg+Mn+Ti+Al^{VI})$	<0.001	<0.001
Muscovite	$Ti/(Fe+Mg+Mn+Ti+Al^{VI})$	0.012	0.005
Amphibole	$Na/(Na+K+\square)$: A site	0.093	0.042
Amphibole	$\square/(Na+K+\square)$: A site	0.883	0.044
Amphibole	$Ca/(Al+Na+Ca)$	0.493	0.012
Amphibole	$Al/(Al+Na+Ca)$	0.442	0.009
Amphibole	$Na/(Al+Na+Ca)$	0.065	0.003

C. Fe-Mg partitioning between coexisting mineral phases.

Mineral i	$K = \dfrac{(Fe/Mg)_{Ch}}{(Fe/Mg)_i}$	Standard deviation of K
Biotite	0.889	0.055
Ankerite	1.815	0.118
Amphibole	0.960	0.044
Muscovite	1.051	0.068
Calcite	0.792	0.070

1C). Observed textures and measured partitioning of Fe and Mg between minerals is consistent with the attainment of chemical equilibrium among phases during the metamorphic episode.

Temperature of metamorphism

Two calibrated mineral thermometers occur: garnet–biotite and calcite–ankerite. Table 2 summarizes compositional parameters of biotite, garnet, and calcite coexisting with ankerite that were used as input for calculations of metamorphic temperatures. The mole fraction of $MgCO_3$ in calcite, when referred to the calibration of Ferry (1976b), based on the experiments of Goldsmith and Newton (1969), indicates equilibrium temperatures of 441°–471°C (±20°) for seven calcite–ankerite pairs. The Fe/Mg ratios of biotite and garnet, when referred to the calibration of Ferry and Spear (1978), indicate equilibration temperatures of 460°–479°C (±50°) for two biotite–garnet pairs. When compositions of biotite–garnet pairs are referred to the geothermometer of Goldman and Albee (1977), equilibration temperatures of 424°–432°C are recorded by the same two biotite–garnet pairs. The temperature at the time of chemical equilibrium during metamorphism at the quarry was near 450°C. In the thermodynamic treatment of phase equilibria that follows, it is assumed that minerals equilibrated at 450°C.

Determination of differences in chemical potentials of volatile components between samples during metamorphism: methods and assumptions

In terms of the system $MgO–FeO–CaO–Al_2O_3–SiO_2–K_2O–Na_2O–C–S–CO_2–H_2O$, considering that all assemblages contain two plagioclase feldspars, assemblages (b) and (d) are trivariant, whereas assemblages (a) and (c) are quadrivariant. The trivariant mineral assemblages plot along curves on isothermal, isobaric μ_{CO_2}–μ_{H_2O} diagrams, whereas the quadrivariant assemblages plot in the regions between the curves. The two isobaric, isothermal univariant curves, along which assemblages (b) and (d) plot, meet at an invariant point (Fig. 5), corresponding to the (unobserved) equilibrium among calcite, ankerite, muscovite, biotite, chlorite, quartz, calcic amphibole, pyrrhotite, graphite, and two plagioclase feldspars. Curves radiating out from the invariant point correspond to mineral reactions among various combinations of these eleven mineral phases. The relative positioning of the curves in Figure 5 was determined by the method of Schreinemakers. The regions of the
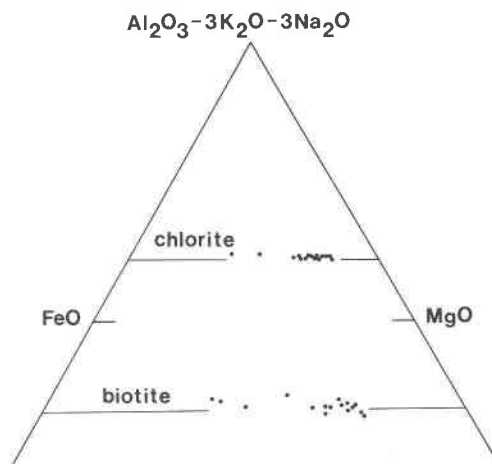

Fig. 3. Compositions of biotite and chlorite plotted on a diagram that projects through SiO_2, H_2O, KAl_3O_5, and $NaAl_3O_5$ (biotite and chlorite coexisting with quartz and muscovite of fixed K/Na under conditions of constant P, T, and μ_{H_2O}). Horizontal lines represent the composition of biotite and chlorite listed in Table 1A.

μ_{CO_2}–μ_{H_2O} diagram in which assemblage types (a)–(d) plot are noted by the letters A, B, C, and D.

Figure 6 illustrates the equilibrium curves from Figure 5 that are pertinent to the observed mineral assemblages; the diagram is drawn to scale. The posi-
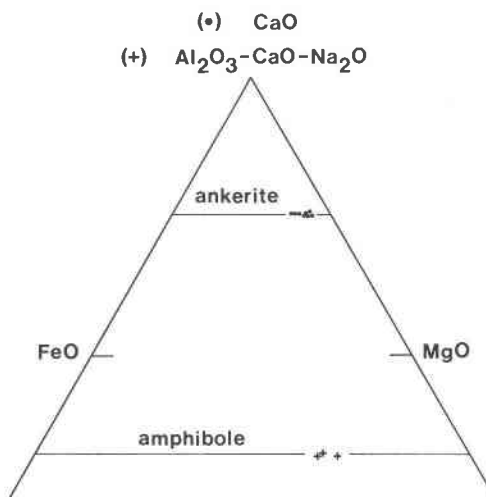

Fig. 4. Compositions of ankerite (circles) on a diagram that projects through CO_2. The ankerite diagram has CaO as the coordinate at the apex of the triangle and refers to conditions of constant T, P, and μ_{CO_2}. Crosses are compositions of calcic amphibole plotted on a diagram with $Al_2O_3–CaO–Na_2O$ as the coordinate at the apex of the triangle. The amphibole diagram projects through SiO_2, H_2O, $CaAl_2O_4$, and $NaAlO_2$ (amphibole coexisting with quartz and plagioclase of fixed composition under conditions of constant P, T, and μ_{H_2O}). Horizontal lines represent the composition of ankerite and amphibole listed in Table 1A.

Table 2. Compositions of coexisting biotite and garnet and of calcite coexisting with ankerite; metamorphic temperatures calculated from compositions of biotite–garnet and calcite–ankerite pairs

A. Composition of calcite coexisting with ankerite; temperature from expression (17) of Ferry (1976b).

Specimen number	Average X_{MgCO_3}	$T(^\circ C)$
5-3	0.037	459
B50	0.039	471
B66	0.042	487
B87A	0.034	441
B87B	0.035	447
B93	0.034	441
B95	0.038	465

B. (Mg/Fe) for coexisting garnet-biotite pairs; temperature from expression (7) of Ferry and Spear (1978) at P = 3500 bars.

Specimen number	(Mg/Fe):garnet	(Mg/Fe):biotite	$T(^\circ C)$
B32	0.111	0.919	460
B43	0.080	0.615	479

tion of the curves in Figure 6 and their segmentation by composition were calculated following the procedure developed by Rumble (1974), which builds upon material presented in lectures by James B. Thompson, Jr. at Harvard University. Details of the calculations are presented in Appendix 2.[1] In summary, the curve labeled D corresponds to the assemblage chlorite + calcite + quartz + amphibole + ankerite + graphite + pyrrhotite + two plagioclases and is the numerical integration of (see Appendix 1 for all notation):

$$4.259(d\mu_{CO_2}/dX_{FeCh}) = -\overline{G}_{FeFeCh}(0.638X_{FeAk}$$
$$+ 0.250X_{FeCh} - 0.865X_{FeAm} - 0.022X_{FeCc}) \quad (1)$$

and

$$8.304(d\mu_{H_2O}/dX_{FeCh}) = -\overline{G}_{FeFeCh}(0.148X_{FeCc}$$
$$+ 2.485X_{FeCh} - 1.416X_{FeAm} - 1.216X_{FeAk}) \quad (2)$$

The curve labeled B in Figure 6 corresponds to the assemblage chlorite + calcite + quartz + muscovite + biotite + ankerite + graphite + pyrrhotite + two plagioclases and is the numerical integration of

[1] To obtain a copy of Appendix 2, order Document AM-79-108 from the Business Office, Mineralogical Society of America, 2000 Florida Ave., NW, Washington, DC 20009. Please remit $1.00 in advance for the microfiche.

$$10.000(d\mu_{H_2O}/dX_{FeCh}) = -\overline{G}_{FeFeCh}(0.144X_{FeCc}$$
$$+ 2.567X_{FeCh} + 0.051X_{FeMu}$$
$$- 1.575X_{FeBi} - 1.189X_{FeAk}) \quad (3)$$

and

$$10.000(d\mu_{CO_2}/dX_{FeCh}) = -\overline{G}_{FeFeCh}(1.826X_{FeAk}$$
$$+ 0.060X_{FeMu} + 0.080X_{FeCh}$$
$$- 1.875X_{FeBi} - 0.092X_{FeCc}) \quad (4)$$

The value of $\overline{G}_{FeFeCh}$ was estimated on the assumption that Fe and Mg mix ideally in the chlorite solid solution, that is:

$$\overline{G}_{FeFeCh} = 4.68RT/[X_{FeCh}(1 - X_{FeCh})]$$
$$= 6723/[X_{FeCh}(1 - X_{FeCh})] \quad (5)$$

at 450°C (Rumble, 1976).

Quadrivariant regions clockwise from the curves labeled B and D are contoured by lines of constant composition. Following Rumble's (1974) treatment of quadrivariant equilibria, the set of contour lines extending from curve D has slope −1.023; the set of contour lines extending from curve B has slope
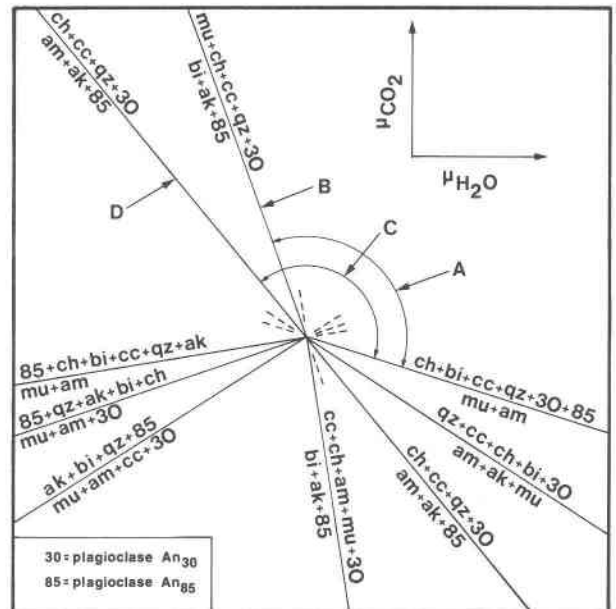

Fig. 5. Equilibria among chlorite, muscovite, biotite, calcite, quartz, ankerite, calcic amphibole, plagioclase An$_{30}$ (30), and plagioclase An$_{85}$ (85) on an isobaric, isothermal μ_{CO_2}–μ_{H_2O} diagram. See Appendix 1 for notation. Phases have compositions listed in Table 1A. Positioning of curves around the invariant point is consistent with the method of Schreinemakers. Assemblage types (a), (b), (c), and (d) occur in parts of the diagram marked by the appropriate letters.
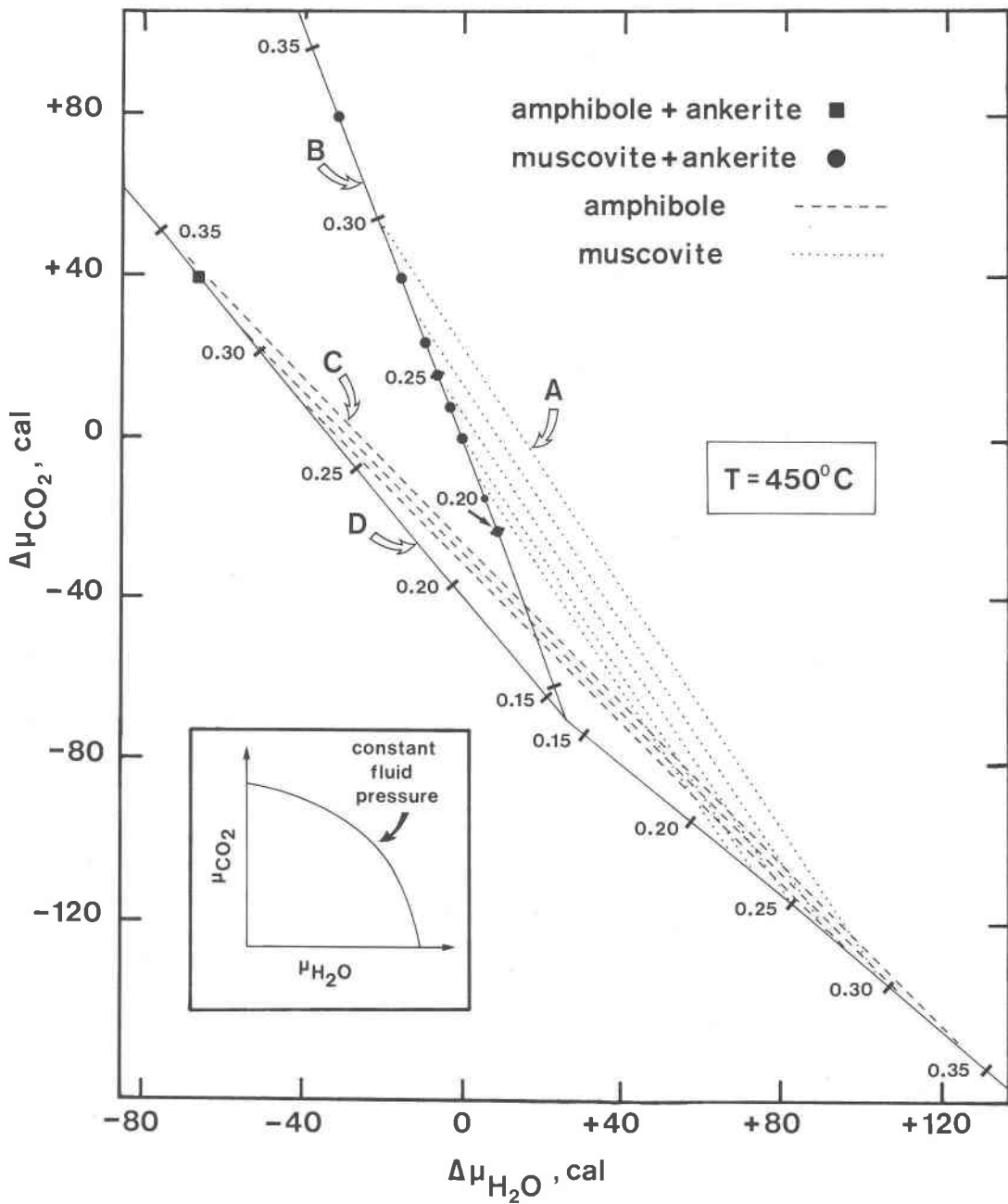
Fig. 6. Quantitative isobaric, isothermal $\Delta\mu_{CO_2}$–$\Delta\mu_{H_2O}$ diagram representing selected equilibria from Figure 5. $\Delta\mu_i = (\mu_i)_{sample}$ – $(\mu_i)_{5-3}$, *i.e.*, the scale is relative to sample 5–3 (0 μ_{CO_2}, 0 μ_{H_2O}). The origin is arbitrarily positioned and as such has no particular significance. Positioning of curves and their segmentation by composition described in the text. The curves are segmented and labeled with values of the composition variable X_{FeCh}. Circles are assemblage type (b); square, assemblage type (d); dotted lines, assemblage type (a); dashed lines, assemblage type (c). Inset illustrates the shape of the loci of points corresponding to a C–O–H–S fluid of constant fluid pressure coexisting with graphite and pyrrhotite of constant composition. Plotted assemblage types are those in Table 3.

–1.536. Assemblage types (a) and (c) lie along these contour lines. The two sets of contour lines in the quadrivariant regions intersect along a third unmarked curve in Figure 6 which corresponds to the

unobserved mineral assemblage muscovite + chlorite + calcite + quartz + calcic amphibole + biotite + graphite + pyrrhotite + two plagioclases. The unmarked curve is the numerical integration of

$$2.187(d\mu_{CO_2}/dX_{FeCh}) = -\overline{G}_{FeFeCh}(1.875X_{FeBi}$$
$$+ 0.028X_{FeCc} + 0.635\ X_{FeCh}$$
$$- 2.476X_{FeAm} - 0.060X_{FeMu}) \quad (6)$$

and

$$1.882(d\mu_{H_2O}/dX_{FeCh}) = -\overline{G}_{FeFeCh}(0.138X_{FeCh}$$
$$+ 0.051X_{FeMu} + 1.384X_{FeAm}$$
$$- 1.575\ X_{FeBi}) \quad (7)$$

The three curves in Figure 6 intersect at an isobaric, isothermal invariant point, and the intersection must occur at $X_{FeCh} = 0.14\pm0.005$ in order for the trivariant curves and the contours in the quadrivariant regions to have a topology consistent with Schreinemakers analysis and to have the proper slopes dictated by equations 1–7.

The only assumptions made in constructing Figure 6 were: minerals have compositions listed in Table 1A; Fe and Mg partition between minerals as listed in Table 1C; pressure is constant; $T = 450°C$; and Fe and Mg mix ideally in chlorite solid solution. The scale in Figure 6 is accurate, but the actual position of the curves in $\mu_{CO_2}-\mu_{H_2O}$ space cannot be determined without thermochemical data. The origin has no particular significance; it has been arbitrarily positioned so that for sample 5-3 $\Delta\mu_{CO_2} = \Delta\mu_{H_2O} = 0$. Values of $\Delta\mu_{CO_2}$ and $\Delta\mu_{H_2O}$ read from Figure 6, therefore, represent differences in μ_{CO_2} and μ_{H_2O} between a specimen of interest and the reference sample 5-3. The tick marks on the trivariant curves represent X_{FeCh} of the chlorite in the mineral assemblage diagrammatically represented by the curve. The composition contours in quadrivariant regions are referred to X_{FeCh}. The compositions of all other phases at any point in the diagram can be reconstructed from the composition of chlorite at that point and the information in Table 1.

Results of determination of differences in chemical potentials of volatile components between samples during metamorphism

The mineral assemblages are plotted in Figure 6 according to the type of mineral assemblage, (a)-(d), and to the composition of chlorite in the assemblage. Table 3 summarizes the assemblages, their location within the quarry, and the composition of chlorite in the particular assemblage. When observed mineral assemblages are plotted on Figure 6, it is apparent that they record differences in μ_{H_2O} and μ_{CO_2} during

metamorphism. At constant temperature and pressure, because the rocks contain graphite and pyrrhotite of constant composition,

$$d\mu_{O_2} = d\mu_{CO_2} - d\mu_C = d\mu_{CO_2} \quad (8)$$

$$d\mu_{CO} = d\mu_C + \tfrac{1}{2}d\mu_{O_2} = \tfrac{1}{2}d\mu_{CO_2} \quad (9)$$

$$d\mu_{H_2} = \tfrac{1}{2}(2d\mu_{H_2O} - d\mu_{O_2}) = \tfrac{1}{2}(2d\mu_{H_2O} - d\mu_{CO_2}) \quad (10)$$

$$d\mu_{CH_4} = d\mu_C + 2d\mu_{H_2} = 2d\mu_{H_2} = 2d\mu_{H_2O} - d\mu_{CO_2} \quad (11)$$

$$d\mu_{S_2} = 0 \quad (12)$$

$$d\mu_{H_2S} = d\mu_{H_2} + \tfrac{1}{2}d\mu_{S_2} = d\mu_{H_2} = \tfrac{1}{2}(2d\mu_{H_2O} - d\mu_{CO_2}) \quad (13)$$

The rocks record differences in the chemical potentials of all major volatile components in the system C–O–H–S present during metamorphism. The magnitudes of the maximum differences (and their estimated error) in terms of both calories and in partial pressures are listed in Table 4 (ideal mixing of components in the volatile phase was assumed in the calculation of the ratios of partial pressures). Errors were estimated by multivariate error analysis (Clifford, 1973), and represent the error in calculated chemical potential differences when an error of $\pm0.01\ X_{FeCh}$ is propagated through the calculations detailed in Appendix 2.

Values of μ_{CO_2} and μ_{H_2O} in calories relative to sample 5-3 are plotted where the samples were collected on a traverse across the north end of the quarry (Fig. 7). Error bars represent the estimated uncertainty in each of the calculated relative chemical potentials. There are no regional trends in μ_{CO_2} or μ_{H_2O} across beds in the quarry. The beds appear to record μ_{CO_2} and μ_{H_2O} values inconsistent with metamorphism at constant activity of volatile components or with metamorphism under some fixed, regionally-controlled gradient in the activity of volatile components perpendicular to the beds.

In Figures 8–10 values of μ_{CO_2} in calories relative to sample 5-3 are plotted where samples were collected along traverses parallel to three beds (1, 2, and 4). Samples collected within each bed differed in their location both in horizontal and vertical dimensions within the quarry. In contrast to samples collected along the traverse across beds, samples collected within a single bed (with the exception of sample 1C) record *no* detectable differences in chemical potentials of CO_2. For example, all samples collected from bed 2 (Fig. 9) are consistent with μ_{CO_2} 14–27 cal less than μ_{CO_2} in sample 5-3; samples collected from bed 4 (Fig. 10) are consistent with μ_{CO_2} 5–11 cal greater than μ_{CO_2} in sample 5-3; samples collected from bed 1

Table 3. Composition of chlorite from metacarbonate rocks collected in the quarry

A. Samples collected along traverse across beds on the north side of the quarry (see text and Figs. 2, 7 for locations).

Specimen number	Assemblage type	$X_{FeCh} (\pm 0.01)$	Specimen number	Assemblage type	$X_{FeCh} (\pm 0.01)$
B4	(b)	0.26	B66	(b)	0.33
B6	(a)	0.22	B72	(b)	0.28
B12A	(a)	0.30	B78	(a)	0.23
B12B	(a)	0.30	B87A	(b)	0.25
B17	(b)	0.23	B91	(c)	0.31
B24	(b)	0.28	B95	(d)	0.33
B47	(a)	0.25	B97	(c)	0.28
B50	(b)	0.24			
B52	(b)	0.20			

B. Samples collected along traverses parallel to beds on the west side of the quarry (see text and Figs. 2, 8, 9, 10 for locations). All samples contain mineral assemblage type (b).

Specimen number	$X_{FeCh} (\pm 0.01)$	Specimen number	$X_{FeCh} (\pm 0.01)$	Specimen number	$X_{FeCh} (\pm 0.01)$
1A	0.30				
1B	0.30	2B	0.20	4A	0.23
1C	0.27	2E	0.21	4B	0.25
1D	0.30	2G	0.20	4C	0.24
1E	0.29				

C. Samples collected from east side of quarry in 1972 - 1973; exact locations unknown.

Specimen number	Assemblage type	$X_{FeCh} (\pm 0.01)$
5-1	(a)	0.27
5-3	(b)	0.23
5-9	(c)	0.34

(with the exception of 1C) are consistent with μ_{CO_2} 46–59 cal greater than μ_{CO_2} in sample 5-3. Sample 1C records μ_{CO_2} that could be as little as 2 cal different from μ_{CO_2} recorded by the other four samples collected in bed 1. From Figure 6 and equations 8–13, it can be seen that if no differences in μ_{CO_2} existed during metamorphism between samples in a single bed, then no differences in the chemical potential of H_2O or of any other C–O–H–S component existed either.

The lack of detectible differences in μ_{CO_2} between samples within individual beds is significant, because differences in μ_{CO_2} between samples were detected in the traverse across beds (see Fig. 7) over distances similar to the lengths of the traverses parallel to beds

(6–10 m). Eleven samples were collected along traverses parallel to beds, but only one of the eleven (1C) is inconsistent with constant μ_{CO_2} during metamorphism within a given bed. In contrast, of the nine samples collected along the traverse across beds plotted in Figure 7, no more than any three samples are consistent with metamorphism at constant μ_{CO_2} across beds.

The data in Figures 7–10 are consistent with a simple pattern of chemical potential differences in three dimensions in the outcrop: differences in the chemical potentials of CO_2, H_2O, and other volatile components of at least 75 calories exist on a scale of less than ten meters in directions that cut across bed-

Table 4. Maximum differences in the chemical potentials of volatile components between rock samples in the quarry

A. Maximum differences in μ_{H_2O}: samples B52 and B95.

i	$(\mu_i)_{95} - (\mu_i)_{52}$ (calories)	$(p_i)_{95}/(p_i)_{52}$
H_2O	-74 ±7	0.95
CO_2	$+63$ ±8	1.04
CH_4	-211 ±22	0.86
H_2	-106 ±11	0.93
O_2	$+63$ ±8	1.04
CO	$+32$ ±4	1.02

B. Maximum differences in μ_{CO_2}: samples B52 and B66.

i	$(\mu_i)_{66} - (\mu_i)_{52}$ (calories)	$(p_i)_{66}/(p_i)_{52}$
CO_2	$+104$ ±12	1.08
H_2O	-39 ±5	0.97
CH_4	-182 ±22	0.88
H_2	-91 ±11	0.94
O_2	$+104$ ±12	1.08
CO	$+52$ ±6	1.04

ding. With the exception of sample 1C, no chemical potential differences have been detected in directions parallel to bedding either in the vertical or horizontal dimension on the same scale of distance. The value of μ_{CO_2} recorded by sample 1C and the error bars in Figures 8–10 indicate that small differences in μ_{CO_2} existed between samples in one bed and may have existed in all beds. Differences in chemical potentials, however, were much smaller within individual beds than were differences in chemical potentials measured between samples collected from different beds.

Differences in the chemical potentials of metal oxide components between samples during metamorphism

In Appendix 2, expressions of the form $(\partial\mu_{CO_2}/\partial X_{FeCh})_{P,T}$ and $(\partial\mu_{H_2O}/\partial X_{FeCh})_{P,T}$ were derived from a thermodynamic analysis of phase equilibria for rock specimens collected. The expressions were then used to compute differences in chemical potentials between samples within the quarry. The same kind of analysis can also be used to derive expressions of the form $(\partial\mu_{MO}/\partial X_{FeCh})_{P,T}$, where μ_{MO} is the chemical potential of metal oxide components in the system $MgO-FeO-CaO-Al_2O_3-K_2O-Na_2O-SiO_2-C-S-$

H_2O-CO_2. Furthermore, the expressions for metal oxide components can be used to compute differences in the chemical potentials of the metal oxide components between rock samples. Although such computations have not been done systematically for all samples, results are presented in Table 5 for two rock pairs. Because all rocks contain quartz, graphite, and pyrrhotite of constant composition, no differences in μ_{SiO_2}, μ_C, or μ_{S_2} existed during metamorphism. Differences in the chemical potentials of MgO, FeO, CaO, Al_2O_3, K_2O, and Na_2O did exist between samples during metamorphism. The magnitude of the chemical potential differences in Table 5 are very similar, with the exception of those for MgO and
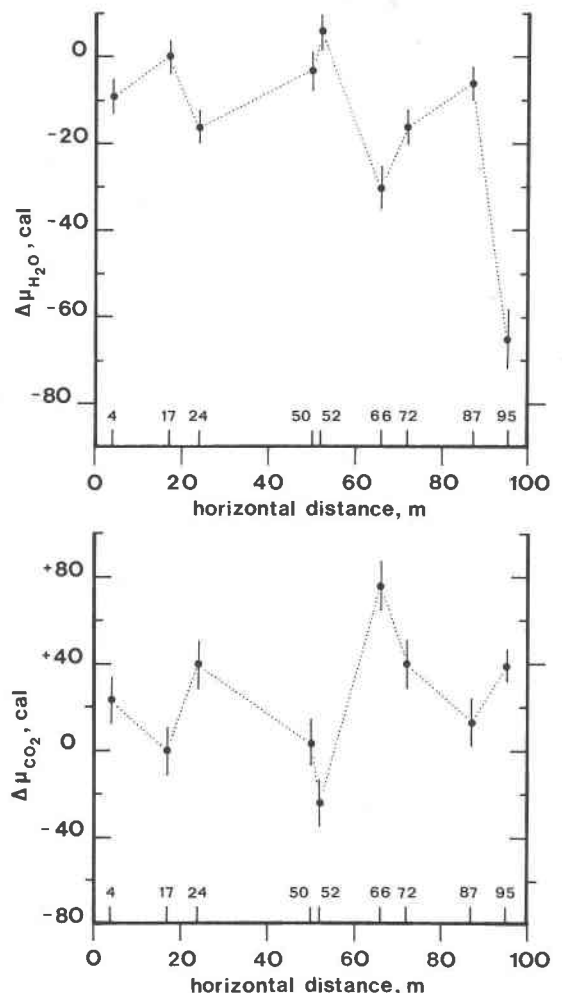

Fig. 7. Differences in μ_{CO_2} and μ_{H_2O} between samples collected along a traverse across layering at the north end of the quarry. $\Delta\mu_i = (\mu_i)_{sample} - (\mu_i)_{5-3}$. Sample numbers at base of the diagram have the "B" prefix omitted. Traverse is located within the quarry in Fig. 2. Vertical bars represent the estimated error in each measured value of $\Delta\mu_i$.
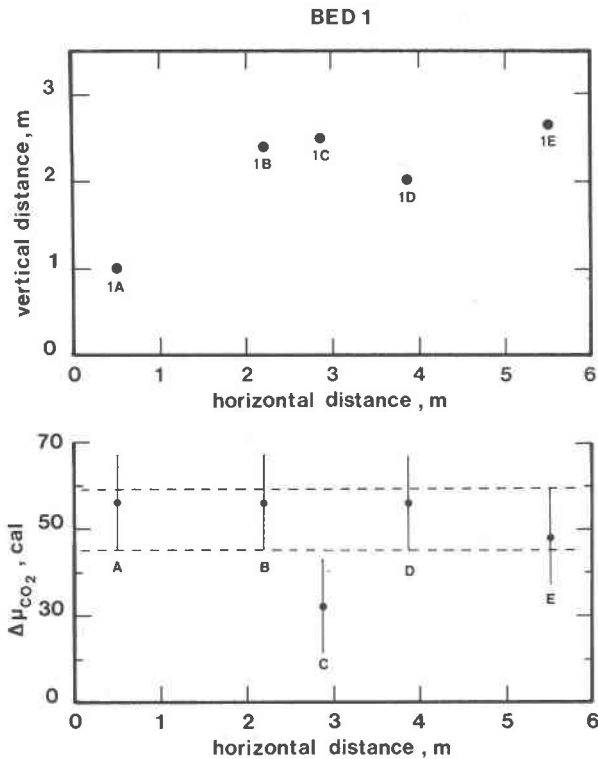
Fig. 8. Top half of the diagram illustrates the relative spacing of samples within bed 1 (see Fig. 2 for location of bed 1). Lower half of the diagram shows $\Delta\mu_{CO_2}$, the difference in μ_{CO_2} between each sample and sample 5–3. Relative position of the samples is projected onto the horizontal axis. Vertical bars represent estimated error in each measurement of $\Delta\mu_{CO_2}$. Except for sample 1C, all samples record the same equilibrium μ_{CO_2} (as well as the same chemical potential of any other component) within error of measurement.

FeO, to the magnitude of the chemical potential differences for CO_2 and H_2O. Differences in the chemical potentials of MgO and FeO between samples are somewhat larger than the differences for the other oxides.

Effect of minor components in mineral solid solutions on calculated chemical potential differences

The mineral formulas in Table 1A are to some degree idealized, and some consideration of minor components neglected in the formulas is in order. The calculated chemical potential differences in Tables 4 and 5 are not large, and it is desirable to demonstrate that neglected minor components in minerals do not have a significant effect on calculated chemical potential differences. Rather than compute the effects of all neglected minor components, two representative minor components are investigated,

and the effect of other minor components is assumed to be similar.

Consideration of a sodium component of muscovite

Analyzed muscovites from rocks collected at the quarry contain a sodium component, $Na(Fe,Mg)_{0.1}Al_{2.8}Si_{3.1}O_{10}(OH)_2$. The mole fraction of this component is reasonably constant in all rocks: 0.056 *esd* 0.018. Chemical potential differences in CO_2 and H_2O were computed using the formula for muscovite, $K_{0.94}Na_{0.06}(Fe,Mg)_{0.1}Al_{2.8}Si_{3.1}O_{10}(OH)_2$, rather than that in Table 1A. Computations are detailed at the end of Appendix 2. The calculated chemical potential differences using a Na-bearing muscovite formula, however, do not differ from differences using a Na-free muscovite composition by more than two percent relative. The neglect of a sodium component in muscovite, therefore, has a negligible affect on the values listed in Tables 4 and 5.

Consideration of a titanium component of biotite

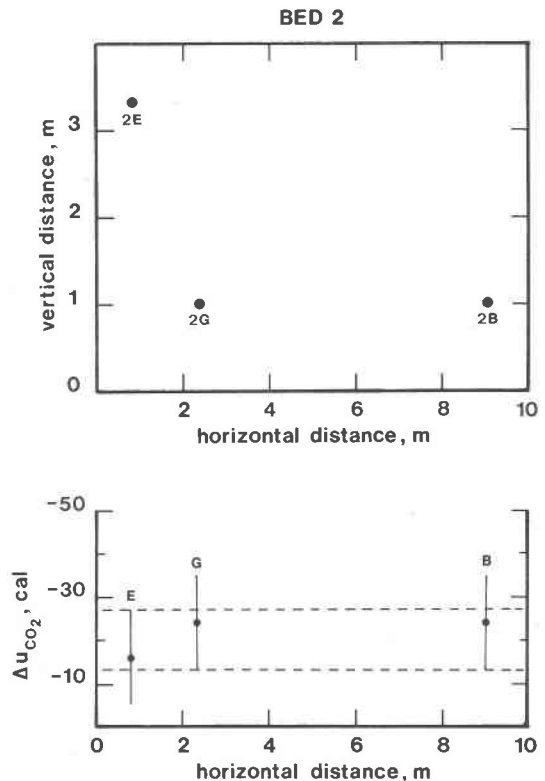The largest neglected minor component in any mineral is the titanium component of biotite. The

Fig. 9. The diagram is identical to Fig. 8 but illustrates relations among samples collected in bed 2. There are no detectable differences in μ_{CO_2} (or the chemical potential of any other component) between samples in bed 2.

BED 4

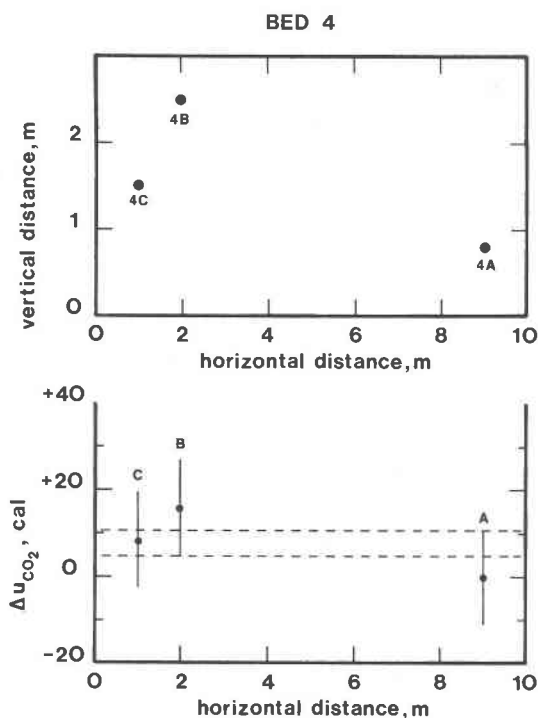Fig. 10. The diagram is identical to Fig. 8 but illustrates relations between samples collected in bed 4. There are no detectable differences in μ_{CO_2} (or the chemical potential of any other component) between samples from bed 4.

atom fraction of Ti in octahedral sites in analyzed biotites is fairly constant: 0.028 *esd* 0.01. If titanium substitutes in biotite by the mechanism $2(Fe,Mg) = Ti\square$, then the titanium component of biotite is $K_{0.9}Ti_{1.375}Al_{1.4}Si_{2.85}O_{10}(OH)_2$. The mole fraction of the titanium component in biotite solid solutions is therefore 0.06 and considered to be constant. Chemical potential differences in CO_2 and H_2O were computed, considering a constant 0.06 mole fraction titanium component in biotite (rather than using the Ti-free biotite formula in Table 1A). Computations are summarized at the end of Appendix 2. The calculated chemical potential differences using the Ti-bearing biotite composition differed from those in Table 4 by no more than two percent relative. The neglect of a titanium-bearing component in biotite, therefore, has only a very small effect on the values listed in Tables 4 and 5.

If Ti in biotite and Na in muscovite are representative of all other neglected minor components, then the neglect of these minor components has not introduced any serious errors into the calculated results summarized in Tables 4 and 5.

Chemical potential gradients during metamorphism

The data presented have been in terms of differences in chemical potentials between samples. Gradients in chemical potentials, however, are the fundamental forces that drive mass transfer by diffusion. Because one of the objectives is to evaluate the geometry of mass transfer of CO_2 and H_2O during metamorphism, gradients in the chemical potentials of CO_2 and H_2O must be evaluated. Chemical potential gradients may be computed from the data in Figures 7–10 by dividing the difference in μ_i between samples by the distance between samples.

The magnitudes of the maximum gradients in μ_{CO_2} and μ_{H_2O} *required* by the data along the traverse across beds are 5.9 cal/m (samples B52 and B66) and 6.0 cal/m (samples B87 and B95), respectively (Fig. 7). Figure 11 shows that the data *permit* much larger chemical potential gradients. For example, the magnitude of the maximum possible gradient in the chemical potential of CO_2 across beds is 27 cal/m between samples B50 and B52. The maximum possible chemical potential gradient is somewhat misleading, because the error bars permit large gradients for closely-spaced samples even when the samples record identical values of calculated $\Delta\mu_i$. Two samples with identical values of measured $\Delta\mu_{CO_2}$ located one meter apart could be consistent with a gradient in μ_{CO_2} of 22 cal/m, simply because the values of $\Delta\mu_{CO_2}$ are uncertain to ±11 cal. Because of the uncertain significance of maximum chemical potential gradients permitted by the data, only chemical potential gradients required by the data will be discussed.

The magnitudes of the maximum required gradients in μ_{CO_2} parallel to beds are much smaller than

Table 5. Differences in the chemical potentials of selected oxide components between rock samples in the quarry in calories

i	$(\mu_i)_{B95} - (\mu_i)_{5-3}$	$(\mu_i)_{B66} - (\mu_i)_{5-3}$
CO_2	+39 ±8	+80 ±12
H_2O	−65 ±7	−30 ±5
CaO	−47 ±11	−88 ±16
MgO	−157 ±29	−198 ±33
Al_2O_3	+47 ±11	+88 ±16
Na_2O	−47 ±11	−88 ±16
K_2O	−8 ±54	−185 ±64
FeO	+588 ±86	+546 ±86
SiO_2	0	0
C	0	0

maximum required gradients in μ_{CO_2} across beds: 0 cal/m (beds 2 and 4)–2.9 cal/m (bed 1). Maximum gradients in μ_{H_2O} parallel to beds are smaller in magnitude: 0 cal/m (beds 2 and 4)–1.1 cal/m (bed 1). If only required chemical potential gradients are considered, maximum gradients in μ_{CO_2} are twice as large across beds as gradients parallel to beds. Maximum gradients in μ_{H_2O} are five times greater across beds than parallel to beds. Note that the existence of any chemical potential gradients parallel to beds is based entirely on one sample (1C, Fig. 8). For two of the beds studied, no gradients in μ_{CO_2} or in μ_{H_2O} can be measured with certainty.

Fluid composition and fluid transfer during metamorphism

Mass transfer of CO_2 and H_2O across beds during metamorphism

The gradients in the chemical potentials of CO_2 and H_2O illustrated in Figure 7 record the existence of forces that would tend to drive mass transfer of CO_2 and H_2O between beds at the quarry site. Mass transfer down chemical potential gradients, however, eventually eliminates the gradients by fluid–mineral reactions that obliterate differences in chemical potentials along the path of mass transfer. The very existence of gradients in μ_{CO_2} and μ_{H_2O} across beds, therefore, can be used to estimate upper limits on the amount of mass transfer of CO_2 and H_2O across beds during some interval of the metamorphic episode.

One upper limit on the amount of mass transfer across beds is the minimum amount of CO_2–H_2O fluid with composition in equilibrium with a particular bed needed to obliterate the mineral assemblages in nearby beds that record values of μ_{CO_2} and μ_{H_2O} different from the chemical potentials in the reference bed. The least upper bound on cross-bed mass transfer of CO_2 and H_2O will be calculated when two samples record large differences in μ_{CO_2} and μ_{H_2O} during metamorphism and when one sample has a small buffer capacity. In this regard, sample B66 is chosen as the reference sample, and sample B52 is paired with it. The least upper bound on cross-bed mass transfer is estimated as the amount of CO_2–H_2O fluid in equilibrium with specimen B66 needed to exhaust the capacity of sample B52 to buffer μ_{CO_2} and μ_{H_2O} at values different from μ_{CO_2} and μ_{H_2O} in B66. Specifically, what is needed to set the upper limit on mass transfer between samples B66 and B52 is: (1) the composition of a CO_2–H_2O fluid in equilibrium with
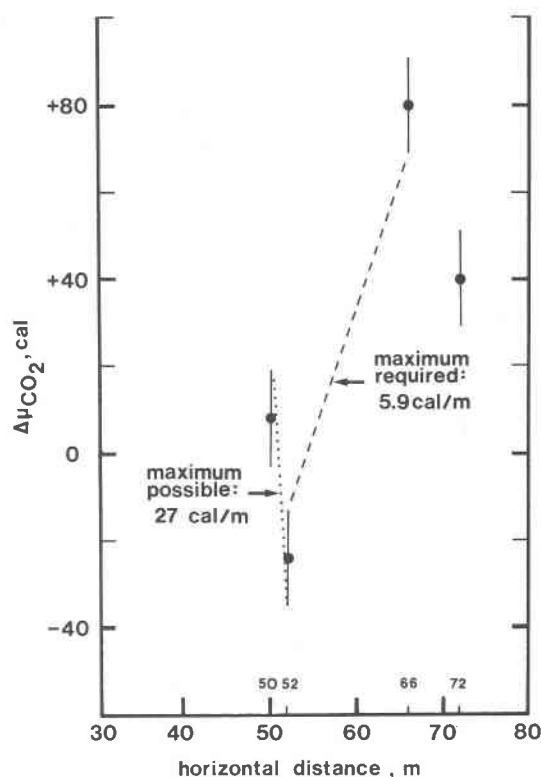

Fig. 11. Enlargement of a portion of Fig. 7 illustrating maximum gradients in μ_{CO_2} across beds permitted (dotted line) and required (dashed line) by the data.

samples B66 and B52 and (2) a formulation of the buffer reaction in sample B52.

Composition of a C–O–H–S fluid in equilibrium with specimen B95. The composition of the fluid in equilibrium with specimen B95 during metamorphism can be estimated from the assemblage ankerite + quartz + calcite + calcic amphibole in the rock. The mineral assemblage records the equilibrium relation:

$$5\mu_{MgAk} + 8\mu_{qz,Qz} + \mu_{H_2O,Fl}$$
$$= \mu_{tr,Am} + 3\mu_{CaCO_3,Cc} + 7\mu_{CO_2,Fl} \qquad (14)$$
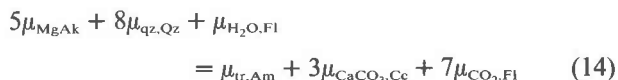
Relation 14 can be quantified using procedures outlined in Ferry (1976b) and numerical expressions in Skippen (1974). The following values of activity were used, estimated from compositions of minerals in B95 and the activity–composition relations of Ferry (1976b): $a_{CaCO_3,Cc} = 0.933$; $a_{MgAk} = 0.762$; $a_{Tr,Am} = 0.0421$. At $T = 450°C$, $p_{H_2O} + p_{CO_2} = P = 3500$ bars. X_{CO_2} of the fluid in equilibrium with the minerals calcite, quartz, ankerite, and calcic amphibole in specimen B95 can be calculated from the numerical equivalent of relation 14. The 3500 bar pressure dur-

ing metamorphism was taken from Ferry (1976b). Calculated $X_{CO_2} = 0.59$.

For completeness, the composition of a C–O–H–S fluid in equilibrium with the minerals in specimen B95 was calculated following the procedure outlined by Ferry (1976b). Fugacity coefficients for components other than CO_2 and H_2O were taken from the tabulation of Ryzhenko and Volkov (1971). Results are summarized in Table 6. A C–O–H–S fluid in equilibrium with the minerals in rock B95 is essentially a CO_2–H_2O fluid: 99.9 mole percent CO_2 + H_2O with $CO_2/(CO_2 + H_2O) = 0.59$.

A second calculation of X_{CO_2} for a fluid in equilibrium with the mineral assemblage in specimen B95 can be made independent of any thermochemical data. Furthermore, X_{CO_2} calculated by this second method is significant because it is made without any assumption regarding the nature of the fluid (*e.g.*, whether it is a gas, liquid, intergranular film, *etc.*). In addition, the estimate is independent of either the temperature or pressure of metamorphism at the quarry. The only assumption made is that CO_2 and H_2O mix ideally in the fluid over the limited range of compositions in equilibrium with samples. The estimate considers sample B95 and any other sample from the quarry. Sample B52 is chosen because differences in chemical potentials of CO_2 and H_2O between these two samples have already been presented (Table 4). If both specimens B95 and B52 were in equilibrium with a CO_2–H_2O fluid, then there are four unknown variables: $(X_{CO_2})_{B95}$, $(X_{H_2O})_{B95}$, $(X_{CO_2})_{B52}$, and $(X_{H_2O})_{B52}$, where numerical subscripts refer to the specimens. Table 4 lists two relations among the four variables: $(p_{CO_2})_{B95}/(p_{CO_2})_{B52} = (X_{CO_2})_{B95}/(X_{CO_2})_{B52} = 1.0448$; $(p_{H_2O})_{B95}/(p_{H_2O})_{B52} = (X_{H_2O})_{B95}/(X_{H_2O})_{B52} = 0.9498$. Although the values of $\Delta\mu_i$ in Table 4 are

temperature-dependent, the ratios of partial pressures (and hence values of X_i) are not. Two other relations, $(X_{CO_2})_{B95} + (X_{H_2O})_{B95} = 1$ and $(X_{CO_2})_{B52} + (X_{H_2O})_{B52} = 1$, allow evaluation of all four variables; specifically $(X_{CO_2})_{B95} = 0.55$, in good agreement with the estimate based on thermochemical data for the equilibrium among ankerite, quartz, calcic amphibole, calcite, and CO_2–H_2O fluid.

Sample B95 may be paired with any other sample from the quarry and X_{CO_2} calculated. Values of $(X_{CO_2})_{B95}$ range from 0.55 to 0.63, in each case supporting the value of 0.59 calculated from thermochemical data.

X_{CO_2} of a fluid in equilibrium with any specimen. Once X_{CO_2} of a fluid in equilibrium with one specimen has been estimated (specifically, B95), X_{CO_2} can be estimated for fluids in equilibrium with all others. If X_{CO_2} of a fluid in equilibrium with the mineral assemblage of bed i is $(X_{CO_2})_i$, then $(X_{CO_2})_i = [(X_{CO_2})_{B95}][\exp (\Delta\mu_i/RT)]$, where $\Delta\mu_i = (\mu_{CO_2})_i - (\mu_{CO_2})_{B95}$ read from Figure 6.

The mineral reaction among muscovite, calcite, quartz, chlorite, ankerite, biotite, plagioclase, and fluid. Finally, the isobaric, isothermal univariant reaction in rocks containing the assemblage muscovite + calcite + quartz + chlorite + ankerite + biotite + two plagioclase feldspars must be evaluated. The exact reaction depends only very slightly on the composition of the minerals involved. For the specific example of the assemblage containing chlorite of $X_{FeCh} = 0.23$, the reaction is

$$3.460Qz + 6.470Cc + 1.999Ch$$
$$+ 2.701Mu + 1.178An_{30} =$$
$$3.001Bi + 1.763Ak + 5.496An_{85}$$
$$+ 7.696H_2O + 2.944 CO_2 \qquad (15)$$

An estimate of the upper limit on the amount of fluid transfer across beds during metamorphism. CO_2–H_2O fluids in equilibrium with samples B52 and B66 are characterized by $X_{CO_2} = 0.5647$ and 0.6071, respectively (if X_{CO_2} of fluid in equilibrium with specimen B95 is 0.590). When a fluid of $X_{CO_2} = 0.6071$ makes contact with sample B52, reaction 15 will proceed in an effort to change X_{CO_2} of the fluid to 0.5647. Reaction 15 will proceed either until the fluid, initially at $X_{CO_2} = 0.6071$, is changed in composition to $X_{CO_2} = 0.5647$ or until the least abundant reactant mineral (chlorite) is exhausted by the reaction. Every 1000 cm^3 of rock B52 contains 8 cm^3 chlorite ($X_{FeCh} = 0.20$), which corresponds to 0.0380 moles chlorite

Table 6. Composition of a C–O–H–S fluid in equilibrium with the mineral assemblage in sample B95. Mole fraction X_{FeS} in pyrrhotite is 0.945. See text for details of the computations
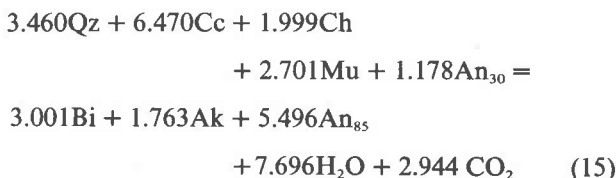
X_{CO_2}	0.59	p_{H_2S}	1.17 bars
p_{CO_2}	2065 bars	p_{H_2}	0.36 bars
p_{H_2O}	1435 bars	p_{CO}	0.49 bars
$\ln f_{S_2}$	−15.635	$\ln f_{SO_2}$	−13.4
$\ln f_{O_2}$	−57.09	$\ln f_{COS}$	−2.62
p_{CH_4}	1.59 bars		

from molar volume data of McOnie *et al.* (1975). A mass balance calculation indicates that 1.374 moles fluid ($X_{CO_2} = 0.6071$) will exhaust 0.0380 moles chlorite through reaction 15. The volumetric fluid–rock ratio needed to destroy the buffer capacity of sample B52 is 49.9 cm³ fluid/1000 cm³ rock = 0.050 (from molar volume data of Burnham *et al.*, 1969 and of Shmonov and Shmulovich, 1974).

The volumetric fluid–rock ratio needed to obliterate the buffer capacity of sample B52 depends on the X_{CO_2} of the fluid with which it comes in contact. In general, for fluids that deviate more greatly from $X_{CO_2} = 0.6071$, the ratio is less than 0.050. For example, if the fluid is pure CO_2 ($X_{CO_2} = 1$), the required fluid–rock ratio is only 0.006. If the fluid is pure H_2O, the fluid–rock ratio is less than approximately 0.001 (depending on the exact location of the curve for reaction 15 on the H_2O-rich side of a T–X_{CO_2} diagram).

Mass transfer of CO_2 and H_2O parallel to beds during metamorphism

The largest difference in μ_{CO_2} that can be measured with certainty between samples in bed 1 is 2 cal (Fig. 8). One upper limit on the amount of mass transfer parallel to beds is the amount of CO_2–H_2O fluid with composition in equilibrium with samples 1A, 1B, 1D, and 1E needed to obliterate the mineral assemblage in sample 1C that buffers μ_{CO_2} at a value 2 cal less than μ_{CO_2} in the other four samples collected in the bed. Samples 1A, 1B, 1D, and 1E are consistent with equilibrium between minerals and a fluid with μ_{CO_2} 46 cal greater than μ_{CO_2} in sample 5-3 (corresponding to a CO_2–H_2O fluid with $X_{CO_2} = 0.5927$). If sample 1C was in equilibrium with a CO_2–H_2O fluid with μ_{CO_2} 44 cal greater than μ_{CO_2} in sample 5-3, the fluid is characterized by $X_{CO_2} = 0.5919$. The least abundant reactant mineral in sample 1C is chlorite, and every 1000 cm³ of rock 1C contains 4 cm³ chlorite ($X_{FeCh} = 0.27$) which corresponds to 0.019 moles chlorite (McOnie *et al.*, 1975). A mass balance calculation indicates that 39.794 moles fluid ($X_{CO_2} = 0.5927$) will exhaust 0.019 moles chlorite through reaction 15. The volumetric fluid–rock ratio needed to destroy the buffer capacity of sample 1C is 1429 cm³ fluid/1000 cm³ rock = 1.429.

Because samples from beds 2 and 4 are consistent with metamorphism at constant chemical potentials of volatile components (no differences in $\Delta\mu_i$ within beds), *any* amount of mass transfer of CO_2 and H_2O could occur along beds 2 and 4, providing the CO_2

and H_2O were contained in a fluid (or fluid-like) phase in equilibrium with the minerals present in beds 2 and 4.

Constraints on the geometry of mass transfer of CO_2 and H_2O during metamorphism

The estimates of upper bounds on mass transfer of CO_2 and H_2O during metamorphism refer to only a specific time portion of the entire metamorphic episode. Because the estimates refer to the buffer assemblages in the rocks discussed, the upper limits on mass transfer apply only to that portion of the rocks' metamorphic history following the formation of the buffer assemblage. Consequently it is difficult to compare the estimated upper limits with other calculations of amounts of fluid transfer during metamorphism. For example, Ferry (1978b) estimated amounts of fluid transfer up to fluid/rock = 0.406 near the quarry, but these values refer to decidedly different metamorphic conditions at higher temperatures close to the granitic stocks in Figure 1. The volume of fluid produced by dehydration–decarbonation reactions in rocks during metamorphism at the quarry site is approximately 230 cm³ fluid/1000 cm³ rock (estimated from the mineralogy of sample 5-3 in Table 7 and the prograde mineral reactions listed by Ferry, 1976a). The volume of fluid derived from dehydration–decarbonation reactions, however, was produced in rocks over an interval of time longer than the time the buffer assemblages in the quarry rocks existed.

In spite of the uncertainty as to whether the estimated upper limits on fluid transfer at the quarry site are large or small relative to actual amounts of fluid transfer during metamorphism, the estimated upper limits on fluid transfer do provide some constraints on the geometry of fluid transfer during metamorph-

Table 7. Modal proportions of minerals in sample 5–3 in volume percent (based on 1000 counted points)

Mineral	Modal percent
Calcite	61.1
Biotite	11.5
Quartz	8.9
Plagioclase	6.6
Muscovite	3.0
Chlorite	0.9
Pyrrhotite	0.5
Graphite	0.7
Ankerite	6.8

ism at the quarry site. During the time interval that the buffer assemblages existed in the rocks at the quarry, if the volume of fluid transfer corresponded to volumetric fluid/rock values of ~0.050 or less, fluid transfer could have occurred in any direction. During the same time interval if fluid transfer were in volumetric amounts of ~0.05 < fluid/rock < ~1.5, then fluid transfer could have occurred parallel to beds but not across beds. Cross-bed fluid transfer of these volumes would have eliminated the chemical potential differences now measured between beds. If fluid transfer in the same time interval were in volumetric amounts of fluid/rock > ~1.5, then fluid transfer could have occurred parallel to some beds (for example, beds 2 and 4) but not others (for example, bed 1).

Because of the uncertainty in the actual amounts of fluid transfer during metamorphism, the data do not *require* any particular geometric pattern of fluid transfer at the quarry site. If fluid transfer occurred in moderate volumes, however, then the transfer must have taken place preferentially in directions parallel to bedding in the quarry. The data are consistent with (but do not require) fluid transfer parallel to bedding even at low volumes of fluid transfer.

Discussion and conclusions

The pattern of chemical potential differences in three dimensions at the quarry site

The differences in chemical potentials of volatile and metal oxide components, estimated from the study of mineralogy and phase equilibria of rocks collected at the outcrop, have a simple, regular geometric pattern. Lithologic layering at the outcrop is vertical and strikes N25E. With the exception of one sample, there are no detectable differences in chemical potentials parallel to layering, either in the horizontal or vertical dimensions. Significant differences in the chemical potentials of components, however, are observed between different layers along a traverse approximately horizontal and perpendicular to the layering. Most differences are on the order of several tens of calories.

Magnitude of observed chemical potential differences relative to other studies

Three other studies (Spear, 1977b; Rumble, 1978; Grew, 1978) have documented chemical potential differences in single outcrops using the same analysis as in this report. Grew, Rumble, and Spear report maximum differences in μ_{H_2O} that are up to one order of magnitude larger than those in this study (300–1200 cal *vs.* 75 cal in Table 4). Grew and Rumble, however, report maximum differences in μ_{O_2} (4500–42,000 cal) that are two orders of magnitude larger than those tabulated in Table 4. The presence of graphite in all rocks of this study accounts for the much smaller differences in μ_{O_2} reported here. Of the three studies, only Rumble reports the distance between samples; for the outcrop he studied, maximum gradients in μ_{H_2O} and μ_{O_2} are 74.7 cal/m and 4902 cal/m, respectively. The gradients reported by Rumble are much larger than the maximum μ_{H_2O} and μ_{O_2} gradients determined from my data (6.0 cal/m and 5.9 cal/m, respectively).

Volatile vs. metal oxide components

Tables 4 and 5 list chemical potential differences in both volatile components (H_2O, CO_2, CH_4, *etc.*) and metal oxide components (MgO, FeO, Al_2O_3, *etc.*). Differences in chemical potentials of metal oxide components are generally similar in magnitude to differences in those of the volatile components. Differences in μ_{FeO} and μ_{MgO}, however, are up to five times greater than differences in the chemical potentials of other components.

Local variations in fluid pressure or in the concentration of non-C-O-H-S components of the fluid during metamorphism

The shape of the loci of points satisfying the condition of constant fluid pressure for a C–O–H–S fluid coexisting with graphite at constant μ_{S_2} is shown in the inset to Figure 6. Samples of assemblage type (b) plot in an array that is consistent with equilibrium with a C–O–H–S fluid (positive differences in μ_{CO_2} between samples are accompanied by negative differences in μ_{H_2O}). The behavior of type (b) assemblages is significant because nowhere in the determination of the μ_{CO_2} and μ_{H_2O} differences was equilibrium with a fluid in any way considered or implied. The pattern of assemblage types (b) and (d), taken together, however, is inconsistent with equilibrium between mineral assemblages and a C–O–H–S fluid of the same fluid pressure. The inconsistency between the array of points in Figure 6 representing the samples from the quarry and the shape of the curve for a C–O–H–S fluid of constant fluid pressure has two possible explanations: first, the thermodynamic analysis does not consider non-C-O-H-S components, such as Na, K, Cl, Ar, and F, that could be in metamorphic fluid.

The presence of these components in the fluid and variation in their concentration from sample locality to sample locality during metamorphism might account for some points in Figure 6 lying off the curve for a C–O–H–S fluid of constant fluid pressure. Second, the mineral assemblages may record differences in fluid pressure during metamorphism. At present there is no way to determine which of the two possibilities is correct.

For two samples 1 and 2, $(\mu_i)_2 - (\mu_i)_1 = RT\ln[(p_i)_2/(p_i)_1]$. The magnitude of the maximum possible differences in fluid pressure or in concentration of non-C–O–H–S components between samples in the quarry can therefore be quantitatively evaluated, where sample 1 is B52 and sample 2 is B66. Lithostatic and fluid pressure during metamorphism in the area was near 3500 bars (Ferry, 1976b). If the value of X_{CO_2} for a fluid in equilibrium with sample B95 is 0.59, the X_{CO_2} of a fluid in equilibrium with sample B66 is also 0.59, corresponding to $p_{CO_2} = 2065$ bars and $p_{H_2O} = 1435$ bars. From the above relation between chemical potentials and partial pressures and the data in Table 3A and Figure 6, the fluid in equilibrium with sample B52 is characterized by $p_{CO_2} = 1927$ bars and $p_{H_2O} = 1471$ bars ($p_{CO_2} + p_{H_2O} = 3398$ bars). Samples B66 and B52 indicate that if differences in fluid pressure between beds did exist during metamorphism, they were approximately 100 bars or less. This fluid pressure difference could likely be supported by the strength of rocks (Brace *et al.*, 1970). If non-C–O–H–S components were contained in a metamorphic fluid of constant fluid pressure, the analysis of samples B66 and B52 indicates that their concentration varied over the outcrop on the order of 0.03 mole fraction or less. For example, if the mole fraction of non-C–O–H–S components in the metamorphic fluid was zero at location B66, it was a maximum of 0.03 at location B52. Quantitative evaluation of maximum differences in fluid pressure and in the concentration of non-C–O–H–S components in the fluid, permitted by the data in Figure 6, indicates that either possibility is a plausible explanation for the inconsistency between the array of data points in Figure 6 and equilibrium of all samples with a C–O–H–S fluid of constant μ_{S_2} and constant fluid pressure.

Physical constraints of fluid transfer during metamorphism

The layering in the quarry is twofold. First, there is vertical, N25E oriented compositional layering (bedding). Second, there is a schistosity imparted by ori-

Appendix 1.   Notation

T	temperature (degrees K except where noted)
P	pressure (bars)
μ_s	chemical potential of system component s (calories)
$\mu_{i,j}$	chemical potential of component i in phase j (calories)
μ_{Fej}	chemical potential of iron end-member of mineral solid solution j in phase j (calories)
μ_{Mgj}	chemical potential of magnesium end-member of mineral solution j in phase j (calories)
X_{ij}	mole fraction of componet i in phase j
X_{CO_2}	$CO_2/(CO_2 + H_2O)$
$\overline{G}_{Ch}$	molar Gibbs energy of chlorite phase (calories)
$\overline{S}_{Ch}$	molar entropy of chlorite phase (e.u.)
$\overline{V}_{Ch}$	molar volume of chlorite phase (calories/bar)
$\overline{S}_{FeCh}$	partial molar entropy of iron end-member of chlorite solid solution (e.u.)
$\overline{S}_{MgCh}$	partial molar entropy of magnesium end-member of chlorite solid solution (e.u.)
$\overline{V}_{FeCh}$	partial molar volume of iron end-member of chlorite solid solution (calories/bar)
$\overline{G}_{FeFeCh}$	$(\partial^2 \overline{G}_{Ch}/\partial X_{FeCh}^2)_{P,T}$
R	universal gas constant (1.987 calories/bar-degree)
P_i	partial pressure of component i (bars)
$a_{i,j}$	activity of component i in phase j
a_{MgAk}	activity of $CaMg(CO_3)_2$ in ankerite solid solution
$\overline{V}_{MgCh}$	partial molar volume of magnesium end-member of chlorite solid solution (calories/bar)

Subscript notation

Phases		Components	
Qz	quartz	Fe	iron end-member of mineral solid solution
Cc	calcite	Mg	magnesium end-member of mineral solid solution
Gr	graphite	tr	$Ca_2Mg_5Si_8O_{22}(OH)_2$
Pl	plagioclase	ab	$NaAlSi_3O_8$
Ch	chlorite	an	$CaAl_2Si_2O_8$
Bi	biotite	qz	SiO_2
Ak	ankerite	Mgak	$CaMg(CO_3)_2$
Mu	muscovite	Mgch	$Mg_{4.68}Al_{2.64}Si_{2.68}O_{10}(OH)_8$
Am	calcic amphibole	Mgcc	$Ca_{0.94}Mg_{0.06}CO_3$
Fl	fluid	Mgam	$Na_{0.2}Ca_{1.9}Mg_{4.05}Al_{1.90}Si_{7.05}O_{22}(OH)_2$
		Ti	titanium end-member of mineral solid solution

Phase notation in Figure 5

ch	$(Mg,Fe)_{4.68}Al_{2.64}Si_{2.68}O_{10}(OH)_8$
cc	$(Mg,Fe)_{0.06}Ca_{0.94}CO_3$
am	$Na_{0.2}Ca_{1.9}(Mg,Fe)_{4.05}Al_{1.9}Si_{7.05}O_{22}(OH)_2$
ak	$Ca(Mg,Fe)(CO_3)_2$
mu	$K(Mg,Fe)_{0.1}Al_{2.8}Si_{3.1}O_{10}(OH)_2$
bi	$K_{0.9}(Mg,Fe)_{2.75}Al_{1.4}Si_{2.85}O_{10}(OH)_2$
30	$Na_{0.7}Ca_{0.3}Al_{1.3}Si_{2.7}O_8$
85	$Na_{0.15}Ca_{0.85}Al_{1.85}Si_{2.15}O_8$
qz	SiO_2

entation of chlorite and muscovite grains parallel to axial planes of folds in the region (also oriented N25E, vertical). Folding in the region, and hence the present orientation of the layering, predated the peak of metamorphism. The layering, therefore, formed natural barriers during the metamorphic event. The three-dimensional pattern of chemical potential differences in the quarry suggests (but does not require) little fluid transfer across layering during metamorphism. The lack of significant chemical potential differences parallel to layering is consistent with any amount of fluid transfer parallel to layering. Fluid transfer during metamorphism may have been controlled, therefore, by sedimentary bedding and (identically-oriented) schistosity. A similar model of fluid transfer has already been presented (Ferry, 1978b), based on a regional study of variations in the volume of fluid transfer during metamorphism.

Acknowledgments

References

Brace, W. F., W. G. Ernst and R. W. Kallberg (1970) An experimental study of tectonic overpressure in Franciscan rocks. *Bull. Geol. Soc. Am., 81,* 1325–1338.

Burnham, C. W., J. R. Holloway and N. F. Davis (1969) Thermodynamic properties of water to 1000°C and 10,000 bars. *Geol. Soc. Am. Spec. Pap. 132.*

Carmichael, D. M. (1970) Intersecting isograds in the Whetstone Lake Area, Ontario. *J. Petrol., 11,* 147–181.

Clifford, A. A. (1973) *Multivariate Error Analysis: a Handbook of Error Propagation and Calculation in Many-parameter Systems.* Wiley, New York.

Ferry, J. M. (1976a) Metamorphism of calcareous sediments in the Waterville–Vassalboro area, south-central Maine: mineral reactions and graphical analysis. *Am. J. Sci., 276,* 841–882.

——— (1976b) P, T, f_{CO_2}, and f_{H_2O} during metamorphism of calcareous sediments in the Waterville–Vassalboro area, south-central Maine. *Contrib. Mineral. Petrol., 57,* 119–143.

——— (1978a) Fluid interaction between granite and sediment during metamorphism, south-central Maine. *Am. J. Sci., 278,* 1025–1056.

——— (1978b) What do mapped isograds tell us about regional patterns of heat transfer and fluid flow during metamorphism? *Geol. Soc. Am. Abstracts with Programs, 10,* 400.

——— and F. S. Spear (1978) Experimental calibration of the partitioning of Fe and Mg between garnet and biotite. *Contrib. Mineral. Petrol., 66,* 113–117.

Finger, L. W. and C. G. Hadidiacos (1971) Aspects of computer automation of an electron microprobe. *Carnegie Inst. Wash. Year Book, 70,* 269–275.

Goldman, D. S. and A. L. Albee (1977) Correlation of Fe/Mg partitioning between garnet and biotite with O^{18}/O^{16} partitioning between quartz and magnetite. *Am. J. Sci., 277,* 750–767.

Goldsmith, J. R. and R. C. Newton (1969) P–T–X relations in the system $CaCO_3$–$MgCO_3$ at high temperatures and pressures. *Am. J. Sci., 267-A,* 160–190.

Greenwood, H. J. (1975) Buffering of pore fluid by metamorphic reactions. *Am. J. Sci., 275,* 573–594.

Grew, E. S. (1978) Oxygen and water gradients in granulite-facies migmatitic pelitic gneisses from Molodezhaya Station, Antarctica (67°40′S, 45°50′E) *Geol. Soc. Am. Abstracts with Programs, 10,* 412.

Guidotti, C. V. (1970) The mineralogy and petrology of the transition from the lower to the upper sillimanite zone in the Oquossoc area, Maine. *J. Petrol., 11,* 277–336.

Hewitt, D. A. (1973) The metamorphism of micaceous limestones from south-central Connecticut. *Am. J. Sci., 273-A,* 444–467.

James, H. L. and A. L. Howland (1955) Mineral facies in iron- and silica-rich rocks. *Bull. Geol. Soc. Am., 66,* 1580–1581.

McOnie, A. W., J. J. Fawcett and R. S. James (1975) The stability of intermediate chlorites of the clinochlore–daphnite series at 2 kbar P_{H_2O}. *Am. Mineral., 60,* 1047–1062.

Osberg, P. H. (1968) Stratigraphy, structural geology, and metamorphism of the Waterville–Vassalboro area, Maine. *Maine Geol. Surv. Bull. 20.*

——— (1971) An equilibrium model for Buchan-type metamorphic rocks, south-central Maine. *Am. Mineral., 56,* 570–586.

——— (1974a) Isochemical metamorphism, south-central Maine. *Trans. Am. Geophys. Union, 55,* 450.

——— (1974b) Buchan-type metamorphism of the Waterville pelite, south-central Maine. In P. H. Osberg, Ed., *Geology of East-central and North-central Maine,* p. 210–222. University of Maine, Orono.

Rice, J. M. (1977a) Contact metamorphism of impure dolomitic limestone in the Boulder aureole, Montana. *Contrib. Mineral. Petrol., 59,* 237–259.

——— (1977b) Progressive metamorphism of impure dolomitic limestone in the Marysville aureole, Montana. *Am. J. Sci., 277,* 1–24.

Rumble, D., III (1974) Gibbs phase rule and its application to geochemistry. *J. Wash. Acad. Sci., 64,* 199–208.

——— (1976) The use of mineral solid solutions to measure chemical potential gradients in rocks. *Am. Mineral., 61,* 1167–1174.

——— (1978) Mineralogy, petrology, and oxygen isotopic geochemistry of the Clough Formation, Black Mountain, Western New Hampshire, U.S.A. *J. Petrol., 19,* 317–340.

Ryzhenko, B. N. and V. P. Volkov (1971) Fugacity coefficients of some gases in a broad range of temperatures and pressures. *Geochem. Int., 8,* 468–481.

Shmonov, V. M. and K. I. Shmulovich (1974) Molal volumes and equation of state of CO_2 at temperatures from 100 to 1000°C and pressures from 2000 to 10,000 bars. *Dokl. Akad. Nauk SSSR, 217,* 206–209.

Skippen, G. B. (1974) An experimental model for low pressure metamorphism of siliceous dolomitic marble. *Am. J. Sci., 274,* 487–509.

Smith, J. V. (1975) Phase equilibria of plagioclase. In P. H. Ribbe, Ed., *Mineralogical Society of America Short Course Notes, vol. 2,* p. Sm1–Sm17. Mineralogical Society of America, Washington.

Spear, F. S. (1977a) Evidence for a miscibility gap in plagioclase feldspar in the composition range An_{39}–An_{88}. *Carnegie Inst. Wash. Year Book, 76,* 619–621.

——— (1977b) Phase equilibria of amphibolites from the Post Pond Volcanics, Vermont. *Carnegie Inst. Wash. Year Book, 76,* 613–619.

Voll, G. (1971) Entmischung von Plagioklasen mit An_{50-55} zu $An_{18} + An_{93}$. *Fortschr. Mineral., 49,* 61–63.